Direct Observation of Current in Type-I Edge-Localized-Mode Filaments on the ASDEX Upgrade Tokamak

N. Vianello,[1] V. Naulin,[2] R. Schrittwieser,[3] H. W. Müller,[4] M. Zuin,[1] C. Ionita,[3] J. J. Rasmussen,[2] F. Mehlmann,[3] V. Rohde,[4] R. Cavazzana,[1] M. Maraschek,[4] and ASDEX Upgrade Team[4]

[1]*Consorzio RFX, Associazione Euratom-ENEA sulla Fusione, Padova, Italy*
[2]*Association EURATOM-Risø DTU, OPL-128 Risø, DK-4000 Roskilde, Denmark*
[3]*Association EURATOM/ÖAW, Institute for Ion Physics and Applied Physics, University of Innsbruck, Innsbruck, Austria*
[4]*Max-Planck-Institut für Plasmaphysik, EURATOM Association, Garching, Germany*

(Received 8 October 2009; published 23 March 2011)

Magnetically confined plasmas in the high confinement regime are regularly subjected to relaxation oscillations, termed edge localized modes (ELMs), leading to large transport events. Present ELM theories rely on a combined effect of edge current and the edge pressure gradients which result in intermediate mode number ($n \cong 10$–15) structures (*filaments*) localized in the perpendicular plane and extended along the field lines. By detailed localized measurements of the magnetic field perturbation associated to type-I ELM filaments, it is shown that these filaments carry a substantial current.

DOI: 10.1103/PhysRevLett.106.125002 PACS numbers: 52.55.Fa, 52.35.Py, 52.70.Ds

Edge localized modes (ELMs) are short (ms) breakdowns of the high confinement regime (H mode), which is envisaged for power producing tokamaks. Because of the high power fluxes, ELMs pose hard to meet demands on the plasma facing components. Thus, insight in and control of ELM events is one of the foremost priorities in fusion research. The interest in ELM physics is enhanced by fascinating analogies with explosive events observed, for example, in solar flares [1] or in magnetic substorms [2].

ELMs are thought to originate from a combination of current and pressure gradient driven MHD modes [3], and result in a medium number ($n \approx$ 10-15) of structures [4–7], localized in the perpendicular plane and extended along the magnetic field. These filaments travel through the scrape-off layer (SOL) and were measured by Langmuir probes on various machines, see, e.g., [8], and observed by high speed cameras [7] or gas puff imaging diagnostic [9].

Magnetic fluctuations associated with ELMs are usually believed to originate from MHD activity. Measurements of magnetic activity were previously performed by magnetic pickup coils close to the vessel wall [7,10] or on insertable probes [11]. These measurements took place far from the filaments, making it difficult to observe the magnetic perturbation of individual filaments and to examine the magnetic fine structure of the ELMs. Both would result in important information such as the excursion of magnetic field lines from their equilibrium position and whether or not the ELMs are associated with reconnection events [1].

Here we report on measurements of type-I ELMs at the ASDEX Upgrade (AUG) tokamak by means of a new probe head (more in [12]). The probe head consists of a cylindrical graphite case (diam = 60 mm) which holds six graphite pins: one measures the ion saturation current, one is swept, the others are floating. Inside the case, 20 mm behind the front side, a magnetic sensor with 1 MHz bandwidth measures the time derivative of the three magnetic field components. A similar probe with combined electrostatic and magnetic signals was already used in AUG [11], but with a wider magnetic coil and a larger distance between electrostatic and magnetic sensors. Our probe was mounted on the midplane manipulator and inserted from the low field side for 100 ms 12 mm inside the limiter position. The data were obtained in type-I ELM-like plasma discharges (nos. 23158, 23159, 23160, 23161, 23163) with a toroidal magnetic field of -2.5 T, 0.8 MA plasma current, 6.5×10^{19} m^{-3} central electron density, and a q_{95} value of 5.2.

We used the ion saturation current to infer the passage of a type-I ELM in front of the probe, as in [13]. In analyzing ELM events we employ the idea that the magnetic signal during the ELM can be separated in frequency. We presume higher frequencies, above few hundred kHz, to be generated mostly by Alfvénic activity or high frequency turbulence. These are not considered here, also because of the frequency cutoff by the graphite shield [12]. Additional MHD activity will still be present at frequencies below 20 kHz, but during ELM filaments most of the signal is presumed to originate from slowly varying currents convected with the filaments. This is justified by the degree of polarization (DOP) analysis [14], which is a test for a plane wave ansatz, quantifying how well the relation $\mathbf{k} \cdot \mathbf{B} = 0$ is satisfied. It is based on the evaluation and diagonalization of the spectral matrix $S = \langle B_i^* B_j \rangle$, calculated in Fourier space. The DOP represents a measure to determine if S represents a pure state, quantifying how well a single eigenvector approximates the state. A high DOP implies that the fluctuations are coherent over several wavelengths. The method can be used to distinguish between propagating modes and coherent localized fluctuations. Figure 1(a) shows the results of DOP analysis. The temporal evolution

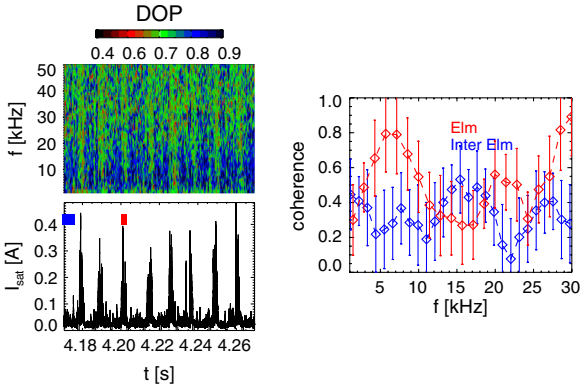

FIG. 1 (color online). Top: Degree of polarization (DOP) as a function of time and frequency. Bottom: Ion saturation current (I_{sat}). Right: Coherence between I_{sat} and b_p computed in ELM and inter-ELM phases. The time intervals are shown in the bottom panel by colored boxes.

of the ion saturation current (I_{sat}) is depicted in the lower panel. A sudden drop in the DOP is observed corresponding to a steep increase of I_{sat}: this implies that the magnetic fluctuations during an ELM can better be represented by coherent structures than by plane wave packets. A coherence analysis between the I_{sat} and the poloidal component of the magnetic field [Fig. 1(c)] reveals an increase of coherence during the ELM activity.

In Fig. 2(b), the increase of magnetic fluctuation amplitude is associated with a change of the phase relation of the radial and poloidal components (b_r and b_p) as highlighted. In particular, the hodogram of the perpendicular magnetic perturbation [Fig. 2(c)], i.e., the magnetic field perturbation trajectory in the b_r-b_p plane, during the passing of the ELM, exhibits a closed orbit at the time interval marked in Fig. 2(b), which is compatible with the passing of current filaments in front of the probe. Outside the ELM the magnetic field perturbation exhibits an almost linear polarization in the perpendicular plane. Thus, magnetic activity in between ELMs (wavelike) differs qualitatively

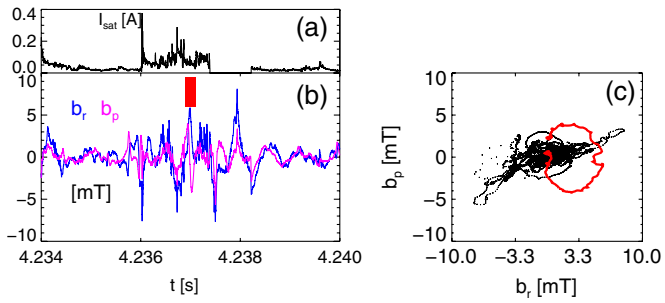

FIG. 2 (color online). (a) Ion saturation current. (b) Poloidal and radial components of the magnetic field. Solid red box highlights the time interval when the two components change their phase relation. (c) Hodogram of radial and poloidal magnetic field components. Closed loop in gray (red) refers to time intervals highlighted in (b).

from the magnetic perturbation during ELMs, which seems to be due to the motion of current filaments.

Measuring all three components of the magnetic perturbation allows checking the alignment of the current filaments directly. In Fig. 3(a) the 3D trajectory of the magnetic field excursion during an ELM event is shown. The time interval is highlighted in Fig. 2. A closed elliptical loop in a plane slightly tilted to the local frame of reference is observed, as expected for filamentary structures. The direction normal to this plane is determined using minimum variance analysis [15]. The method is based on the solution of the eigenvalue problem $\sum_{\nu=1}^{3} M^B_{\mu\nu} n_\nu = \lambda n_\mu$, where $M^B_{\mu\nu} = \langle B_\mu B_\nu \rangle - \langle B_\mu \rangle \langle B_\nu \rangle$ is the magnetic variance matrix, the brackets indicating the mean values averaged over the time the structure spends traveling in front of the probe, μ, $\nu = 1, 2, 3$ denoting the Cartesian components of the system, λ and n being the eigenvalues-vectors of the system, respectively. The eigenvectors represent the direction of maximum, intermediate, and minimum variance of the magnetic field, respectively. The eigenvector n_3 corresponds to the direction of minimum variance and is normal to the plane spanned by the magnetic field perturbation. This direction is parallel to the equilibrium magnetic field [Fig. 3(a), blue line]. This confirms the hypothesis that the ELM filament is aligned with the equilibrium magnetic field. From the sense of polarization the current direction is found to be collinear with the plasma current.

The method allows the determination of the rotation matrix, so that the hodogram in the plane perpendicular to the current filaments may be reconstructed. This is shown in Fig. 3(b) together with a fit to an ellipse. The shape of the hodogram calculated in the rotated frame of reference can be used to determine the type of current distribution associated with an ELM. Theories proposed ELM filaments with monopolar [4,16] or bipolar currents [17]. Up to now no clear evidence of one mechanism predominant with respect to the other was reported. Figure 3(c) shows the anticipated shape of the hodogram in bipolar and monopolar cases. In a bipolar case the hodogram exhibits a cardioidlike shape with a cusp at the origin. This is not recognized in the experimental data [see Fig. 3(b)]. We note that a bipolarlike hodogram with the presence of a cusp was previously recognized in [18] [cf. Fig. 3(b)] where it was associated with a direct measurement of a bipolar current. The filaments observed in [18] are induced by drift-Alfvén turbulence [19]. Further, while a monopolar current hodogram regularly occupies two quadrants, the bipolar one always spans three quadrants: this latter behavior is not observed in the experimental data as can be verified by comparing Figs. 3(b) and 3(c). These results make us confident that the magnetic fluctuations observed are indeed generated by a monopolar current distribution. Under this assumption the current carried by a filament may be estimated. In the rotated frame of reference for a circular monopolar symmetric filament

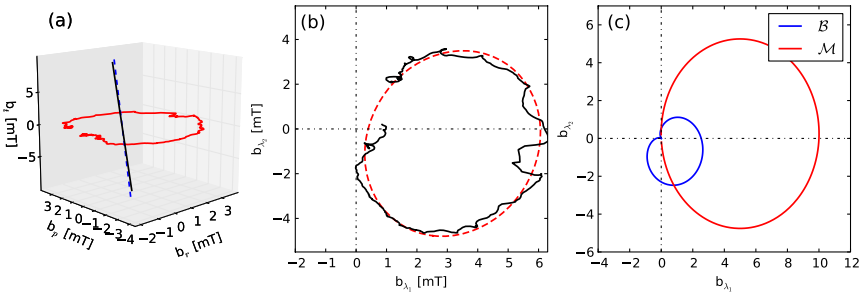

FIG. 3 (color online). (a) Trajectory of ELM filament associated magnetic field excursions in all three spatial directions. Direction of minimum variance is shown (black line) together with direction of equilibrium field (dashed blue line). (b) Hodogram of magnetic perturbation associated with ELM current filament reconstructed in the maximum variance plane. Dashed red line shows the elliptical fit. (c) Hodograms calculated for a monopolar current distribution ($\mathcal{M}$) and bipolar one ($\mathcal{B}$).

drifting in the λ_1 direction, the two perpendicular magnetic field components may be written as $b_{\lambda_1} = \frac{-r_0 B_0 a}{\lambda_1^2 + a^2}$ and $b_{\lambda_2} = -\frac{r_0 B_0 \lambda_1}{\lambda_1^2 + a^2}$, where $B_0 = \frac{\mu_0 I_0}{2\pi r_0}$ and a is the distance between the filament's center and the probe, representing also the distance of closest approach, r_0 is the filament radius, and I_0 its current. The distance a can be approximated, assuming the filament to propagate with a constant velocity in the λ_1 direction: $a = \Delta t v_{\lambda_1}$, where Δt is the time delay between the maximum of b_{λ_1} and the maximum or minimum of b_{λ_2}, where b_{λ_1} and b_{λ_2} are the projections of the magnetic field in the maximum-intermediate variance plane. Thus, within these approximations the current may be estimated noting that $|b_{\lambda_2}(\lambda_1 = a)| = \frac{1}{2}\frac{\mu_0 I_0}{2\pi a} = \frac{\mu_0 I_0}{4\pi \Delta t v_{\lambda_1}}$. From the experimental data we compute the quantities depicted in Fig. 4(a), where Δt was calculated both at the maximum and minimum of b_{λ_2}. The two values Δt_1 and Δt_2 are equal to 38 and 42 μs, respectively. The estimate of the current relies on the knowledge of the local velocity in the λ_1 direction. This propagation was reported for the ASDEX Upgrade tokamak, e.g., [11,20]. The experimental setup does not allow a reliable local measurement of v_r or v_p, neither can we rely in the presented shots on correlation analysis of wall mounted probes (which are 160° separated from the manipulator in the toroidal direction). As best approximation for radial propagation, we thus assume the most probable value $v_r = 1.2$ km/s as determined in [20] and calculate $v_{\lambda_1} = v_r / \cos[\angle(\lambda_1, r)]$, where $\angle(\lambda_1, r)$ is the angle between λ_1 and the radial direction which for the present case is of the order of 7°. From [20] we also estimate a standard deviation of v_r as $\sigma_{v_r} = 700$ m/s, which ensures that 71% of the events are observed within $(v_r \pm \sigma_{v_r})$. With these values the average distance of closest approach is approximately 4 cm, and using the average value between the minimum and maximum of b_{λ_2} we obtain an estimate of 1.9 kA. The total perpendicular field $\sqrt{b_{\lambda_1}^2 + b_{\lambda_2}^2}$ is shown in Fig. 4(b). The magnetic field variation can be fitted by a function of the form $f = [(\alpha/\sqrt{(t - t_0)^2 + \beta}) - \gamma] \times e^{-(t-t_0)/\tau_e}$, t_0 being the time instant of the maximum of the total perpendicular field and τ_e the e-folding time, and assuming the magnetic field to be the response of a passing monopolar current filament. The good quality of the fit provides additional support for the monopolar nature of the filament, also compared with the fit expected from a bipolar current distribution shown with a blue line exhibiting a higher χ^2 [Fig. 4(b)]. The average decay time is determined as $\tau_e \approx 200$ μs. In order to increase the statistic reliability of the previous estimate we have analyzed events from five different shots with similar conditions. The results are shown in Fig. 5. In Fig. 5(a) the joint probability distribution function (PDF) of the independent experimental values Δt and b_{λ_2}, used for the current evaluation, is shown, highlighting how the bulk of the filaments have values of approximately 25 μs and 5 mT. In Fig. 5(b) the histogram of the angle between λ_1 and the radial direction is shown, showing that the λ_1 direction is a complex combination of radial and poloidal propagation. Finally, in Fig. 5(c) the current estimated according to the aforementioned formula is plotted versus the position of the filaments with respect to the separatrix, taking into account the position of the manipulator and the estimated distance of closest approach. The errors represent the influence of the velocity uncertainty on the estimates of a and consequently on I. The bulk of the distribution of these filaments is thus observed in the SOL, even taking into account the uncertainty on v_r: the median of the distribution of the filaments

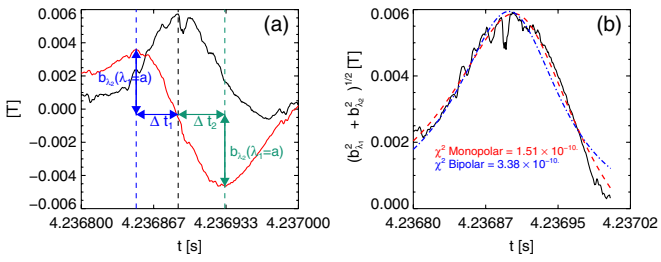

FIG. 4 (color online). (a) Time traces of the two perpendicular components of magnetic field during an ELM filament. (b) Total perpendicular magnetic field as function of time. Superimposed results of a fit for an expected monopolar (red) and bipolar (blue) current distribution both modulated by an exponential decay.

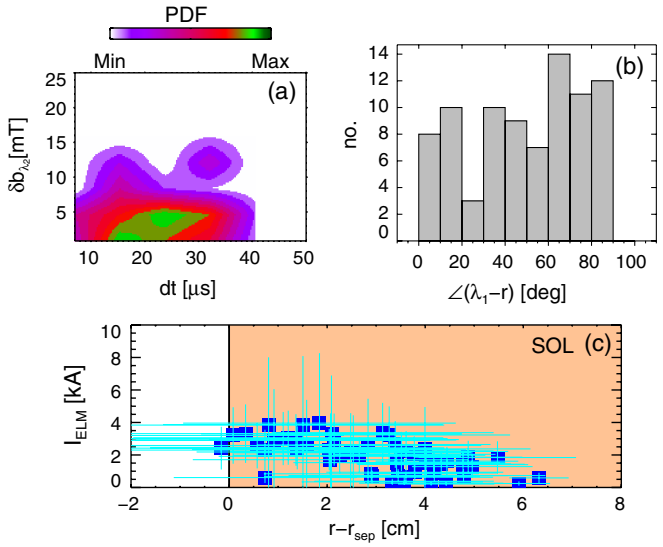

FIG. 5 (color online). (a) Joint PDF of Δt and b_{λ_2} ($\lambda_1 = a$). (b) Histogram of the angle between λ_1 and the radial direction. (c) Filament's current estimate versus distance from the separatrix estimated with $v_r = 1.2$ km/s. Error bars result from propagation of velocity uncertainty in the estimate of a and I.

in the SOL within the error in their position is 1.4 kA, corresponding to a $j_{\parallel} \approx 4.5$ MA/m^2 for 1 cm radius filaments. These values are consistent with measurements of edge currents, e.g., in [21]. It was supposed in [22] that, if the ELM breakdown is driven by peeling instabilities, the ELM will lead to a flattening of the current density profile over the separatrix and an increase of currents flowing into the SOL. These currents will be nearly force-free and accompanied by poloidal halo currents closing through the divertor tiles. Actually, these currents were measured [12,23] with values up to few tens of kA, supporting the presence of rapid flow of toroidal currents from the plasma into the SOL. The resulting histogram may also be compared with the estimate for ELM filaments in JET tokamak given in [24]: in this case the most probable current was of the order of 450 A, but with a lower radial velocity postulated. For completeness it must be noted that the same current density was estimated in [11], assuming the magnetic perturbation to be induced by a rotating helical structure with a bidirectional current close to, but still inside, the separatrix. The value found is higher than the measured j_{sat} current density to the ion-biased pin (≈ 50 kA/m^2).

Concluding this Letter, we have provided evidence that ELM filaments carry considerable currents for which we found reasonable estimates. The magnetic signals during ELM filaments differ substantially from wave activity in between ELMs. We have shown that the current in the filaments is coaligned to the plasma current and the magnitude expected for the edge. The current flows along the unperturbed magnetic field lines and has a unidirectional nature. This poses the question of where the filament currents close in the SOL and why such high current densities are sustained in the ELM filaments. We hope that future experiments will contribute to answer these questions, which will shed new light on the instability mechanisms for ELMs.

This work is supported by the European Communities under the contract of Associations between EURATOM and ENEA, Risø DTU, ÖAW Innsbruck, and IPP Garching, and by project P19901 of the Austrian Science Fund (FWF).

[1] W. Fundamenski *et al.*, Plasma Phys. Controlled Fusion **49**, R43 (2007).
[2] A. Lui, IEEE Trans. Plasma Sci. **28**, 1854 (2000).
[3] P. B. Snyder, H. R. Wilson, and X. Q. Xu, Phys. Plasmas **12**, 056115 (2005).
[4] A. Kirk *et al.*, Plasma Phys. Controlled Fusion **48**, B433 (2006).
[5] M. Fenstermacher *et al.*, Nucl. Fusion **45**, 1493 (2005).
[6] A. Herrmann *et al.*, J. Nucl. Mater. **363–365**, 528 (2007).
[7] A. Kirk *et al.*, Phys. Rev. Lett. **96**, 185001 (2006).
[8] A. W. Leonard *et al.*, Plasma Phys. Controlled Fusion **48**, A149 (2006).
[9] R. Maqueda, R. Maingi, and NSTX team), Phys. Plasmas **16**, 056117 (2009).
[10] H. Takahashi, E. D. Fredrickson, and M. J. Schaffer, Phys. Rev. Lett. **100**, 205001 (2008).
[11] A. Herrmann *et al.*, in *Proceedings of the 22nd Energy Fusion Conference, Geneva, 2008* (IAEA, Vienna, 2008), p. EX/P6-1.
[12] C. Ionita *et al.*, J. Plasma Fusion Res. Series **8**, 413 (2009).
[13] M. Endler *et al.*, Plasma Phys. Controlled Fusion **47**, 219 (2005).
[14] J. Samson and J. Olson, Geophys. J. Int. **61**, 115 (1980); O. Santolík, Radio Sci. **38**, 13 (2003).
[15] D. R. Weimer, J. Geophys. Res. **108**, 12 (2003).
[16] J. R. Myra, Phys. Plasmas **14**, 102314 (2007).
[17] V. Rozhansky and A. Kirk, Plasma Phys. Controlled Fusion **50**, 025008 (2008).
[18] M. Spolaore *et al.*, Phys. Rev. Lett. **102**, 165001 (2009).
[19] N. Vianello *et al.*, Nucl. Fusion **50**, 042002 (2010).
[20] A. Kirk *et al.*, Plasma Phys. Controlled Fusion **53**, 035003 (2011).
[21] D. Thomas *et al.*, Phys. Plasmas **12**, 056123 (2005).
[22] E. Wolfrum *et al.*, in *Proceedings of the 22nd Energy Fusion Conference, Geneva, 2008* (Ref. [11]), p. EX/P3-7.
[23] P. McCarthy *et al.*, in *Proceedings of the 30th European Physical Society Conference on Plasma Physics, St. Petersburg, 2003* (EPS, St. Petersburg, 2003), Vol. 27A, p. P-1.064.
[24] P. Migliucci and V. Naulin, Phys. Plasmas **17**, 072507 (2010).